Liquid Crystals
Publication details, including instructions for authors and subscription information:
http://www.informaworld.com/smpp/title~content=t713926090

Study of different modes of dielectric relaxation in a newly synthesized material exhibiting ferro-, ferri- and antiferro-electric phases

M. B. Pandey[a]; R. Dhar Corresponding author[a]; V. K. Agrawal[b]; R. Dabrowski[c]; M. Tykarska[c]
[a] Physics Department, Ewing Christian College, Allahabad-211 003, India [b] Physics Department, Allahabad University, Allahabad-211 002, India [c] Institute of Chemistry, Military University of Technology, 00-908 Warsaw, Poland

Online publication date: 25 May 2010

To cite this Article Pandey, M. B. , Dhar Corresponding author, R. , Agrawal, V. K. , Dabrowski, R. and Tykarska, M.(2004) 'Study of different modes of dielectric relaxation in a newly synthesized material exhibiting ferro-, ferri- and antiferro-electric phases', Liquid Crystals, 31: 7, 973 — 987
To link to this Article: DOI: 10.1080/02678290410001709275
URL: http://dx.doi.org/10.1080/02678290410001709275

LIQUID CRYSTALS, VOL. 31, NO. 7, JULY 2004, 973–987

Study of different modes of dielectric relaxation in a newly synthesized material exhibiting ferro-, ferri- and antiferro-electric phases

M. B. PANDEY, R. DHAR*
Physics Department, Ewing Christian College, Allahabad-211 003, India

V. K. AGRAWAL
Physics Department, Allahabad University, Allahabad-211 002, India

R. DABROWSKI and M. TYKARSKA
Institute of Chemistry, Military University of Technology, 00-908 Warsaw, Poland

(*Received 21 October 2003; in final form 23 February 2004; accepted 5 March 2004*)

Employing thermodynamical, optical and comprehensive dielectric studies, we have investigated a freshly synthesized chlorinated MHPOBC analogue antiferroelectric liquid crystal; it exhibits different chiral SmC sub-phases, viz. SmC^*_α, SmC^* and SmC^*_γ, at considerably lower temperature in comparison with MHPOBC, and a wide range room temperature antiferroelectric SmC^*_A phase. Dielectric spectroscopy investigations under planar molecular anchoring were carried out in the frequency range 1 Hz to 10 MHz. The data measured for low and high frequency regions were corrected by the method of fitting operation of the theoretical equations. Seven different modes of dielectric relaxation in the different phases were identified. Soft mode relaxation was identified in the SmA^* and SmC^*_α phases. The Goldstone mode, characteristic of the ferroelectric phase, was observed in the SmC^* and SmC^*_γ phases. Two characteristic peaks are seen in the spectrum of the SmC^*_A phase: one, at high frequency, corresponds to fluctuation where the molecules in neighbouring layers are rotating in opposite phase; the other, at low frequency, arises due to phase fluctuation in the helicoidal superstructure.

1. Introduction

Antiferroelectricity in a chiral liquid crystal was first reported by Chandani *et al*. in MHPOBC [1]. Antiferroelectric liquid crystals (AFLCs) are polar smectic liquid crystals in which the direction of tilt and spontaneous polarization in neighbouring layers point in the opposite direction, implying a lack of macroscopic spontaneous polarization in their antiferroelectric (SmC^*_A) phase [2]. In these materials, competition between the adjacent smectic layers to form anticlinic and synclinic structures causes the appearance of different chiral smectic C subphases, viz. SmC^*_α, SmC^*_β and SmC^*_γ, with distinct macroscopic properties in a narrow temperature region in addition to the SmC^*_A phase [2]. The most general phase sequence, with lowered temperatures, is SmA^*–SmC^*_α–SmC^*–SmC^*_β–SmC^*_γ–SmC^*_A [3, 4]. In a sample of high optical purity, i.e. in material consisting of molecules of single absolute conformation, SmC^*_β and SmC^*_γ phases exist directly below the SmC^*_α phase, and disappear in favour of an ordinary synclinic SmC^* phase with an excess of enantiomer of opposite handedness [3]. In a particular system certain intermediate phases can be absent, but if they exist they always appear in the above sequence [4, 5]. The SmC^*_α phase has an incommensurate structure with a modulation period between five and eight smectic layers, while the unit cells of the SmC^*_β, SmC^*_γ and SmC^*_A phases consist of four, three and two smectic layers, respectively [6]. The SmC^*_α phase shows antiferroelectric-like properties at higher temperatures and changes to a ferroelectric-like structure on cooling [7]. Recently Gorecka and co-workers [3] have been able to solve the long known controversy concerning the ferroelectric and ferrielectric nature of the SmC^*_β (sometimes

*Author for correspondence;
e-mail: dr_ravindra_dhar@rediffmail.com

Liquid Crystals ISSN 0267-8292 print/ISSN 1366-5855 online © 2004 Taylor & Francis Ltd
http://www.tandf.co.uk/journals
DOI: 10.1080/02678290410001709275

denoted as SmF_{I2}^{*}) phase. They have shown that in the optically pure antiferroelectric liquid crystal MHPOBC, the SmC_{β}^{*} phase is neither ferrielectric nor ferroelectric, but has antiferroelectric properties with a four-layer structured unit cell; this has been identified in several other AFLC compounds and denoted as an AF phase [8–11]. The SmC_{γ}^{*} phase has ferrielectric nature and its periodic unit consists of three smectic layers, in two of which the molecules tilt in the same direction while in the third layer they tilt in the opposite direction [12, 13].

Since their discovery, AFLCs have attracted much attention due to their potential application to new fast switching displays [2, 14], and also from the need to understand their fundamental structure and properties. Up to now a large number of AFLCs have been synthesized and intensively studied by means of dielectric spectroscopy [7–11, 15–19], electro-optic anlaysis [20–22], X-ray diffraction [6] and conoscopy [23]. Only a few compounds have so for been reported to show the SmC_{A}^{*} phase with a broad temperature range near room temperature which is a basic requirement for the application of these materials to display devices. Recently more such materials have been found among compounds with fluorinated terminal chains [24]. The existence and structure of SmC* subphases is not yet fully understood and is still a matter of discussion. In recent years it has become clear that the experimental conditions under which the materials are studied may affect the phase behaviour to an extant previously not commonly recognized [4]. In particular, a strong surface influence may produce not only a geometrical difference from the bulk phases, but also a large shift in phase transition temperatures, phase coexistence and in some cases even complete exclusion of phases [4, 25].

The groups of Furukawa *et al.* [26] and Sasaki *et al.* [27] have previously reported the synthesis of chlorinated MHPOBC, 4′-octyloxybiphenyl-4-carboxylic acid 3-chloro-4-(1-methylheptyloxycarbonyl)phenyl ester:

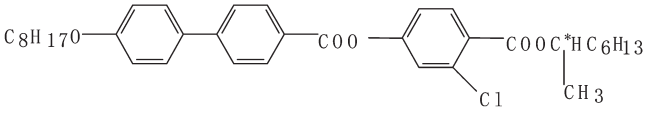

Furukawa *et al.* [26] reported an I (116.3) SmA* (97.0) SmC* (94.9) SmY* (29.5°C)Cr phase sequence whereas Sasaki *et al.* [27] reported I (120.0) SmA* (57.0) SmC* (50.0°C)Cr on the basis of calorimetry and polarizing microscopy. In view of these different numbers of phases with different temperature ranges reported by two independent groups on chlorinated MHPOBC, and the presence of SmC* subphases (SmC_{α}^{*}, SmC_{β}^{*} and SmC_{γ}^{*}) and the SmC_{A}^{*} phase in MHPOBC [1, 3, 4], we were tempted to resynthesize chlorinated MHPOBC with special care to maintain optical purity, and then to study the effect of chlorination on the sequence of phases, their temperature range of existence and dielectric behaviour. Optical purity of the resynthesized chlorinated *S*-MHPOBC is better than 99.5%. In the present work we have performed a comprehensive dielectric study besides the most frequently used calorimetry and polarizing optical microscopy to determine the phases of chlorinated MHPOBC.

2. Experimental techniques

The various mesophase transition temperatures and transition enthalpies were determined by differential scanning calorimetry (DSC) (Setaram, model DSC 141). A transmitted light polarizing microscope was used to identify the textures of the different mesophases. The nature of the mesophases was confirmed by miscibility studies as well. Helical pitches were measured by selective reflection of light in a cell treated for homeotropic sample alignment, using a Varian-Cary 3E UV–Vis spectrophotometer.

Dielectric studies of planar aligned samples were carried out in the frequency range 1 Hz to 10 MHz using a Solartron SI-1260 impedance/gain phase analyser, coupled with a Solartron dielectric interface model-1296. Planar alignment of the molecules was achieved by depositing a thin layer of polyamide nylon onto ITO-coated glass electrodes (sheet resistance $\sim 25\,\Omega$) and then rubbing the electrodes unidirectionally with soft cotton. The two plates of the dielectric cell were separated by mylar spacers of thickness 20 μm. The temperature of the sample for optical and dielectric studies was controlled by a hot stage (Instec, model HS-1) with an accuracy of ± 0.003°C. The temperature near the sample was determined by measuring the thermo-emf of a copper–constantan thermocouple using a six and a half digit multimeter. A measuring electric field of $0.1\,V_{rms}$ was applied across the sample in a direction parallel to the smectic layers. The heating cycle was performed from the SmC_{A}^{*} phase as it was not possible to crystallize the sample at room temperature (lowest value ~ 18°C). Other details of experimental techniques have been discussed elsewhere [28, 29].

To analyse the measurement data, the dielectric spectra were fitted with the help of the generalized Cole–Cole equation [30]:

$$\varepsilon^{*} = \varepsilon' - \mathrm{i}\varepsilon'' = \varepsilon'(\infty) + \sum_{i} \frac{(\Delta\varepsilon)}{1 + (\mathrm{i}\omega\tau_i)^{(1-h_i)}} + \frac{A_1}{\omega^{n}} + \frac{\sigma(\mathrm{d.c.})}{\mathrm{i}\varepsilon_0\omega} \quad (1)$$

where $\varepsilon'(\infty)$ is the relative permittivity at the high frequency limit; $\Delta\varepsilon_i$, τ_i and h_i are the dielectric strength, relaxation time (inverse of angular relaxation frequency) and symmetric distribution parameter

($0 \leqslant h_i \leqslant 1$) of the ith mode, respectively. The third and fourth terms in equation (1) represent the contribution of electrode capacitance and ionic conductance at low frequencies where A_1 and n are constants [31, 32]. σ(d.c.) is the ionic conductance and ε_0 ($=8.85\,\mathrm{pF\,m^{-1}}$) is the free space permittivity. The measured dielectric absorption ε'' contains a spurious contribution above 10 kHz due to the finite resistance of ITO-coated electrodes [32, 33]. An additional imaginary term Af^m [32] is added in equation (1) to account partially for the ITO effect; A and m are constants as long as correction terms are small. The high frequency impedance model proposed by Gouda *et al*. [32] has been modified by adding a lead inductance (L) of the cell in series to the resistance of the ITO coating (R) [33]. The modified high frequency impedance model explains the dielectric spectrum of an empty (air-filled) cell and a cell filled with non-dispersive materials, quantitatively; whereas the dielectric spectrum of a cell filled with dispersive material is explained qualitatively. The factor A in the case of a cell filled with dispersive material depends on R, L, C, G and the reactive cut-off frequency ω_{x0} of the cell in a complex manner. The reactive cut-off frequency of the cell is given as [33]

$$\omega_{x0} = \omega_0 \left[1 - \left(\frac{LG^2}{C}\right)\right]^{\frac{1}{2}} \qquad (2)$$

where G and C are the a.c. conductance and capacitance of the filled dielectric cell and $\omega_0 = 1/(\mathrm{LC})^{\frac{1}{2}}$.

The characteristic parameters of all the relaxation modes in different phases have been calculated by fitting equation (1) to the experimental data with the help of a computer program using Origin Software. The results of the fitting procedure are shown in figure 1, and are in good agreement with the measured curve.

Instrumental uncertainty in the determination of transition temperatures and transition enthalpies ΔH by DSC are $\pm 0.1^\circ$C and $\pm 5\%$, respectively. The accuracy in measurement of capacitance C and conductance G in the frequency range concerned is $<0.2\%$, and hence the maximum uncertainty in the measurement of dielectric permittivity $\varepsilon'_\perp$ and dielectric loss $\varepsilon''_\perp$ within the entire frequency range is less than $\pm 1\%$. The accuracy of measured frequency is ± 100 ppm. The uncertainty in estimation of relaxation frequency, dielectric strength and distribution parameter in SmA* and chiral smectic C subphases is well within $\pm 10\%$, while the uncertainty in the estimation of the distribution parameter near the SmA*–SmC$^*_\alpha$ transition increases to $\pm 20\%$. In the SmC$^*_\mathrm{A}$ phase, uncertainty in the determination of relaxation frequency is less than $\pm 10\%$ for both modes, but uncertainties in the determination of dielectric strength and distribution parameter increase to $\pm 50\%$ due to the weak dielectric strength, the broad nature of relaxation peaks and the small capacitance in this phase.

3. Results and discussion

3.1. *Phase transitions and textures*

DSC thermograms during heating and cooling at a rate of $0.2^\circ\mathrm{C\,min^{-1}}$ are shown in figure 2 (*a*). Transition temperatures and corresponding transition enthalpies are given in the table. On heating, the sample melts at 26.4°C (Cr–SmC$^*_\mathrm{A}$) and enters the isotropic liquid phase at 117.3°C, showing SmC* subphases and an SmA* phase in between. During cooling, all the phases are reproduced, the SmC$^*_\mathrm{A}$ phase showing a large supercooling. It was not possible to record a SmC$^*_\mathrm{A}$–Cr transition on DSC thermogram down to −20°C; however, the sample did crystallize after leaving it overnight several degrees below ambient temperature. To examine crystallization, we cooled the material just after melting figure 2 (*b*), and found that it has a tendency to crystallize at about 0°C under these conditions. Figure 2 (*c*) shows an expanded thermogram on the section of temperature scale representing transitions between different chiral smectic C subphases. DSC peaks corresponding to SmC$^*_\mathrm{A}$–SmC$^*_\gamma$, SmC$^*_\gamma$–SmC* and SmC$^*_\alpha$–SmA* are clearly observed, while the SmC*–SmC$^*_\alpha$ transition appears as a shoulder but it is clear enough to represent the transition. The effect of the chlorination of MHPOBC on the sequence of phases and their temperature ranges is seen clearly in the table. It is notable that all the phases have considerably shifted towards lower temperatures. The SmC$^*_\mathrm{A}$ phase has shifted to room temperature and that also has a wide temperature range.

Figure 3 shows the optical textures of different phases on cooling the sample from isotropic phase in a cell in which the bounding surfaces are coated with lecithin for homeotropic orientation; the alignment, however, is not perfect. Textures are analogous to those of an unaligned sample. A completely dark field of view was observed in all phases in case of the perfect homeotropic alignment, but only after shearing the two cell-plates in the SmA* phase. Taking the sample to the isotropic phase disturbs the alignment. The SmC$^*_\alpha$ phase appears similar to the SmA* phase, except that the colour of the focal-conic fans becomes yellowish, and some parallel lines appear on the fans, figures 3 (*a*) and 3 (*b*). At the SmC$^*_\alpha$–SmC* transition, the colour of the fans tends towards green spectrum and the parallel lines become wrinkled. Dechiralization lines also appear towards the lower temperature side of SmC* phase, see figure 3 (*c*). We observed a pitch variation in the SmC* phase from 400 nm at higher temperatures to 426 nm towards lower temperatures, see figure 4. At the SmC*–SmC$^*_\gamma$ phase transition, due to the drastic

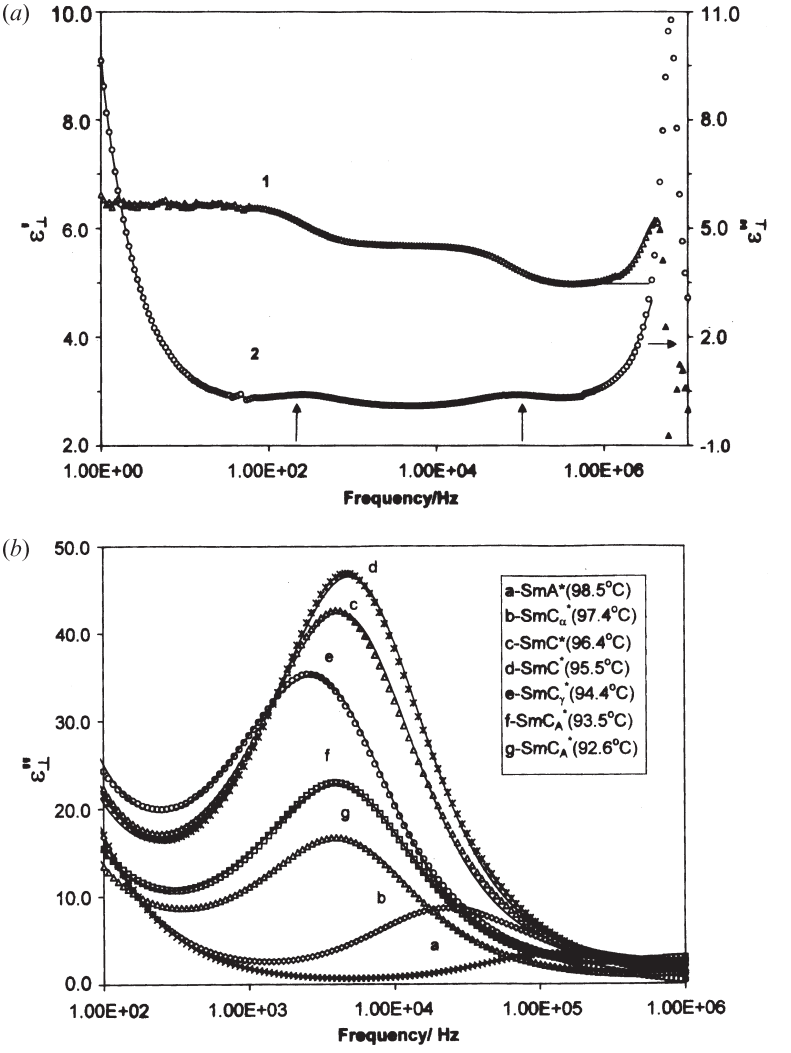

Figure 1. (*a*) An example of data analysis (mode separation) by simulation of experimental data using equation (1). Curves 1 and 2 show the frequency dependence of dielectric permittivity $\varepsilon'_\perp$ and dielectric loss $\varepsilon''_\perp$, respectively, in the antiferroelectric SmC^*_A phase at 31.8°C. Open symbols represent experimental data, while solid lines represent fitted curves. Two relaxation modes present in the SmC^*_A phase are marked by vertical arrows. (*b*) Dielectric absorption spectra in the SmA^*, SmC^*_α, SmC^* SmC^*_γ and SmC^*_A phases. The solid lines represent the fitting of equation (1) to the experimental data in the different phases. Data below 100 Hz and above 1 MHz are influenced by low and high frequency effects, respectively, and are not shown here, in order to enhance the visualization of transitions between different chiral smectic subphases.

increase of pitch, widely spaced lines appear, figure 3 (*d*). It was not possible to measure pitches in the SmC^*_γ phase as this was beyond the instrumental limit (900 nm) and therefore we speculate that it is in the range of a few microns, as observed for some other materials [12, 21]. At the onset of the SmC^*_A phase, band lines slowly disappear, figure 3 (*e*). It was possible to measure the pitch of the SmC^*_A phase below 95.0°C, where it is 386 nm, increasing to 618 nm at 30.0°C. The colour change in optical textures, and the appearance of dechiralization lines, are more pronounced in the cells where the bounding surfaces are not alignment treated.

From optical texture studies, the following phase sequence was observed: I (116.8) SmA^*(99.0) SmC^*_α (98.5) SmC^*(96.3) SmC^*_γ(96.0°C) SmC^*_A. We could not achieve crystallization (or melting) because the cell was not cooled below ambient temperature ($\sim$18°C), to avoid contamination of the sample due to the trapping of the water vapour, etc. Transition temperatures obtained from optical texture studies and DSC are similar; however, a noticeable difference is seen between the transition temperatures obtained from the plots of the various dielectric parameters (discussed below) and those obtained from DSC/optical texture studies. Several other workers have also reported such differences [11, 13, 18, 20], which are not surprising

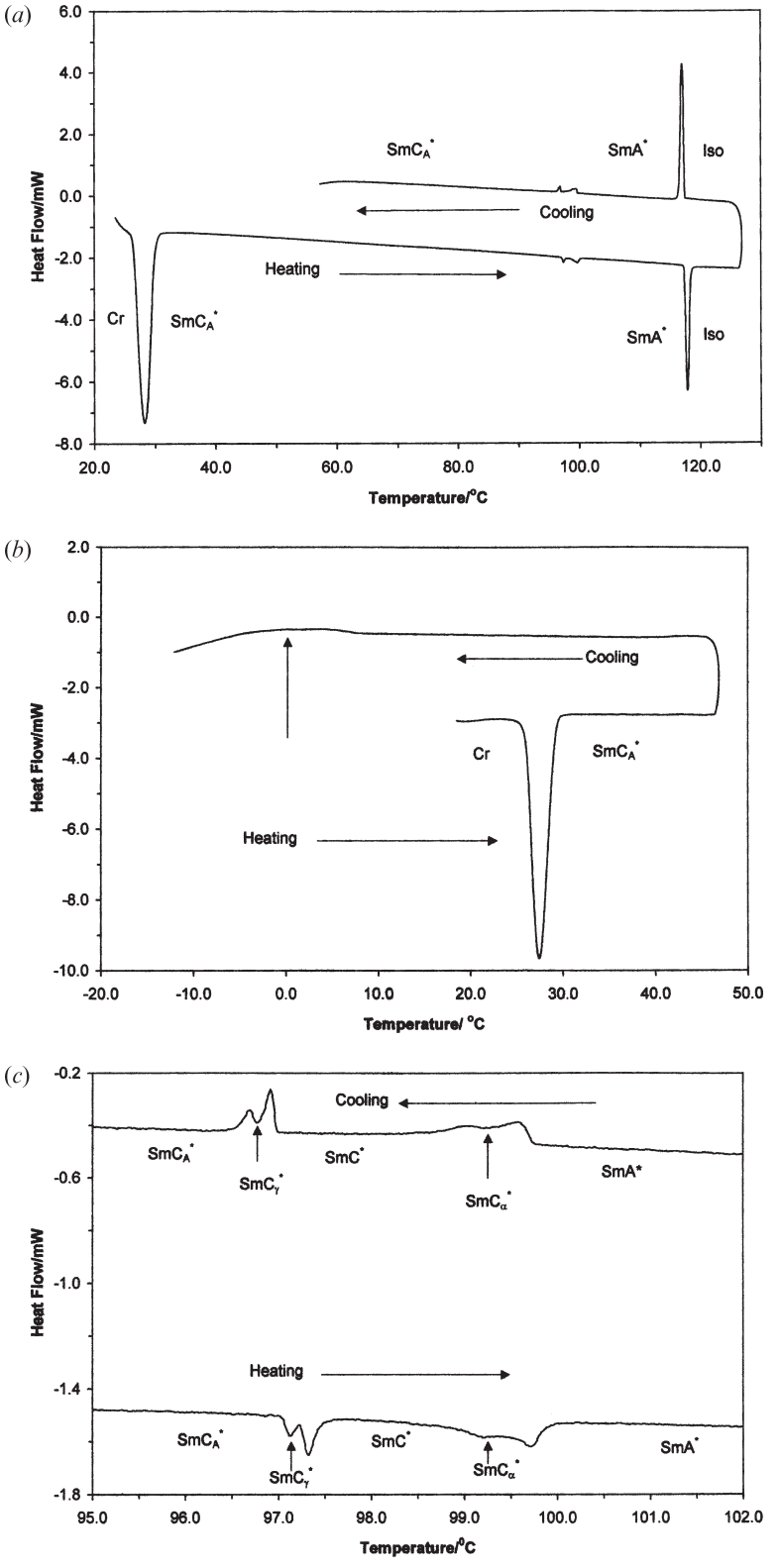

Figure 2. (*a*) DSC thermogram for heating and cooling cycles at a scanning rate of $0.2^\circ C\,min^{-1}$. (*b*) DSC thermogram showing the cooling of the sample from the SmC_A^* phase. Under these conditions a slow crystallization process is visible at about 0°C (marked by a vertical arrow), which is not observed when cooling from the isotropic liquid. (*c*) DSC thermogram on an expanded temperature scale representing transitions between different chiral smectic C subphases.

Table. Phase transition temperatures (°C) and transition enthalpies (cal mol^{-1}) (in parentheses) of chlorinated MHPOBC, *S*-MHPOBC(Cl), obtained from DSC during heating and cooling, and reported transition temperatures (°C) of MHPOBC.

Compound	Cr	•	SmC_A^*	•	SmC_γ^*	•	SmC^*	•	SmC_α^*	•	SmA^*	•	I
S-MHPOBC(Cl)		26.4		97.03		97.22		98.85		99.37		117.27	
(Heating)		(4240)		(6.90)		(14.09)		(12.56)		(22.46)		(947)	
S-MHPOBC(Cl)		—		96.79		96.98		99.49		99.76		117.4	
(Cooling)				(−7.76)		(−14.36)		(−7.88)		(−26.57)		(−943)	
S-MHPOBC[a]	Cr82.7 (SmI_A^* (65.3)) SmC_A^*118.2 SmC_γ^*119.1 SmC_β^*120.0 SmC_α^*121.9 SmA^*147.6 I.												
R-MHPOBC	Cr 84 SmC_A^*118.4 SmC_γ^*119.2 SmC_β^*120.9 SmC_α^*122 SmA^*148 I (from [15]).												
R-MHPOBC	Cr 31 SmI_A^*66 SmC_A^*117.5 SmC_γ^*119.3 SmC^*121.5 SmC_α^*123.2 SmA^*145 I (from [13]).												

[a]R. Dabrowski, unpublished data.

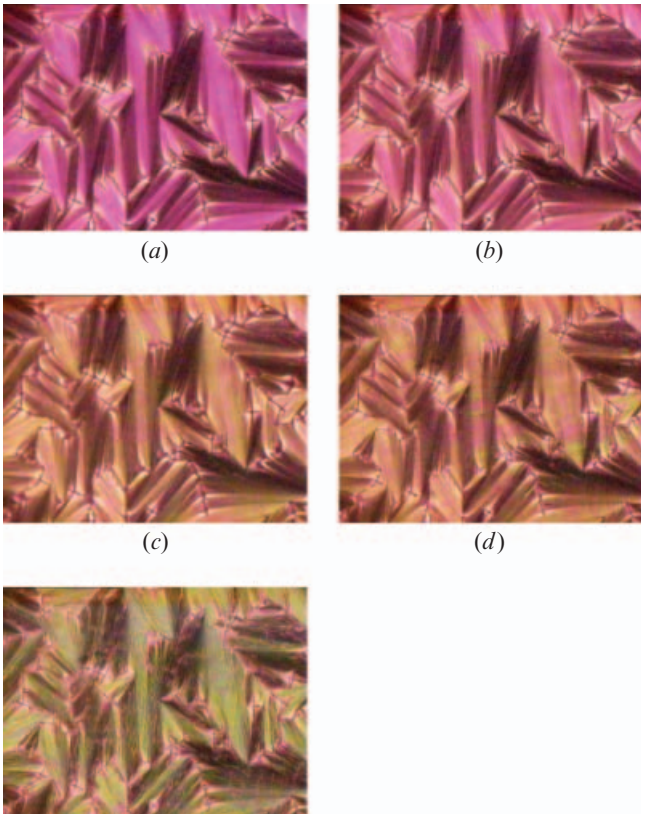

Figure 3. Optical textures (100×) of various phases under crossed polarizers for an unaligned sample (10 μm); bounding surfaces of the cell are coated for homeotropic alignment. (*a*) SmA^* (99.5°C), (*b*) SmC_α^* (98.6°C), (*c*) SmC^* (97.0°C), (*d*) SmC_γ^* (96.3°C) and (*e*) SmC_A^* (93.2°C). Perfect homeotropic alignment in the SmA^* phase is observed only if the bounding surfaces are sheared, and then a completely dark field of view is observed for all the phases.

because the appearance of these phases and transition temperatures are sensitive to sample history, surface conditions and thickness of the sample [4, 25]. The mode of temperature change during the experiment may also be responsible for observed differences in transition temperatures. In the case of DSC and optical texture studies, temperature variation is dynamic even though small (~0.2°C min^{-1}), but in the dielectric study the temperature variation is quasi-static.

3.2. *Dielectric permittivity*

The temperature dependence of dielectric permittivity of the different phases at various frequencies is shown in figure 5, where the dielectric behaviour of five liquid crystalline phases, viz. SmA^*, SmC_α^*, SmC^*, SmC_γ^* and SmC_A^*, can be easily distinguished. Below 100 Hz, the value of $\varepsilon'_\perp$ increases with decrease in frequency due to the contribution of electrode polarization capacitance and ionic conductance at all temperatures [31, 32]. In the SmA^* phase the value of $\varepsilon'_\perp$ is small and remains constant throughout the phase. A sharp increase was observed in $\varepsilon'_\perp$ in the vicinity of the SmC_α^* phase. The maximum value of $\varepsilon'_\perp$ has been found to be more than 125 at 100 Hz in the SmC^* phase, during both heating and cooling, which is due to the large spontaneous polarization in this phase [2]. It was observed that $\varepsilon'_\perp$ increases cycle by cycle, showing that the SmC^* phase develops at the expense of the antiferroelectric SmC_β^* phase [3, 4]; however, we could not observe an antiferroelectric SmC_β^* phase (seen in MHPOBC) in any cycle. In the SmC_γ^* phase, $\varepsilon'_\perp$ decreases smoothly with decrease in temperature due to the decrease in ferroelectric ordering in this phase [12]. In the SmC_A^* phase, $\varepsilon'_\perp$ was found to be quite small (~5) in comparison with other polar SmC^* subphases, due to the opposite tilting of the molecules in adjacent smectic layers, and remains unchanged throughout the phase. Hiraoka *et al.* [15] have reported a maximum value of $\varepsilon'_\perp$ at about 100 at 1 kHz in the SmC^* and ~25 in the SmC_α^* phase for pure *R*-MHPOBC. The values of $\varepsilon'_\perp$ in the present material are higher in all the mesophases in comparison with MHPOBC.

The temperature range of the SmC_α^* phase is rather narrow, ~0.5°C (see figure 2), and it is difficult to recognize SmA^*–SmC_α^* and SmC_α^*–SmC^* transitions in the dielectric measurements. Due to first order

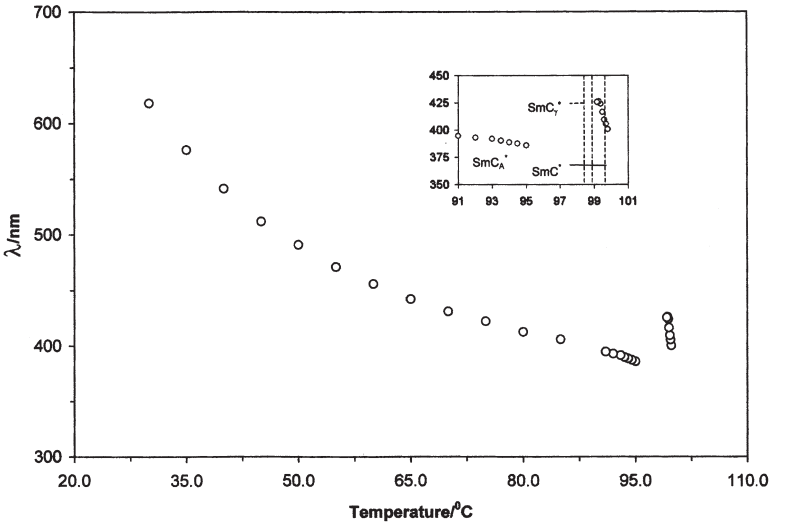

Figure 4. Temperature dependence of the helical pitch for a homeotropic aligned 100 μm thick sample measured by the selective reflection method ($p = 1.3\ \lambda$).

nature of the transition [3] and small temperature gradient in the cell which is difficult to avoid in a sample of large electrode area, the SmC$_\alpha^*$ phase may co-exist with adjacent phases. For this reason it is difficult to conclude whether the value of $\varepsilon'_\perp$ in the SmC$_\alpha^*$ temperature range is actually that of pure SmC$_\alpha^*$ phase or is a consequence of the coexistence of SmC* and SmC$_\alpha^*$ phases, thus typical for the synclinic ferroelectric SmC* phase. The DSC thermogram also suggests that there may be a coexistence of SmC* and SmC$_\alpha^*$ phases (see figure 2). Carvalho *et al.* [18] have reported a maximum value of $\varepsilon'_\perp$ in the SmC$_\alpha^*$ phase to be about ~ 60 in a compound having a thiobenzoate group with flouro-substitution; Sarmento *et al.* [7] have reported the same value in the fluorinated compound 11HFBBM7.

The slightly higher value of $\varepsilon'_\perp$ in the SmC$_\alpha^*$ phase of the present material, as compared with MHPOBC, may be the effect of chlorination. However, it should be noted that the vertical lines of figure 5 show the separation of different phases on the basis of DSC data, and these lines may not represent actual transitions from dielectric study. To identify the locations of these lines, I–SmA* transition temperatures obtained from DSC and dielectric studies have been normalized and the difference incorporated in all the transition temperatures obtained by DSC. If we take DSC/optical texture transition temperature without normalization, then the value of $\varepsilon'_\perp$ in the SmC$_\alpha^*$ phase is not more than 10–12. One possibility for clearing the doubt is the simultaneous observation of optical texture and dielectric measurement, but unfortunately no change in texture at the SmA*–SmC$_\alpha^*$ transition could be seen in the planar sample.

3.3. *Relaxation modes*

The Cole–Cole plots of the different relaxation modes observed in various phases are depicted in figure 6. The data points lie on a semicircle except for those at lower and higher frequencies. The corrected data points diverge from measured data points due to the dominating low and high frequency correction terms present in the experimental data, even in the middle frequency range. Low frequency effects due to ionic conductance [31, 32] are present up to ~ 10 kHz. Data above 10 kHz are affected by the finite resistance of ITO sheet and the lead inductance, indicating that high frequency effects are exceptionally dominating in this cell. In many other cells containing non-ferroelectric materials, the high frequency effect starts only above 100 kHz [33]. In general it has been observed that high frequency correction starts nearly two decades of frequency below the reactive cut-off frequency (ω_{x0}) of the cell [33]. In the chiral smectic C sub phases, the reactive cut-off frequency of the sample cell shifts towards lower frequency, due to the large capacitance, see equation (2); hence the high frequency correction term starts below 100 kHz in these phases.

In the SmC$_A^*$ phase, the high frequency correction term is expected to start above 100 kHz because of the higher reactive cut-off frequency in comparison with ferroelectric phases, and the same results have been observed in our cell. Because on cooling the sample, the low frequency effect decreases with decrease in temperature, corrected data points in the SmC$_A^*$ phase follow measured data points in the middle frequency region, and only small correction terms are present at lower and higher frequencies. From figure 6 it is evident that the dielectric strength of the relaxation

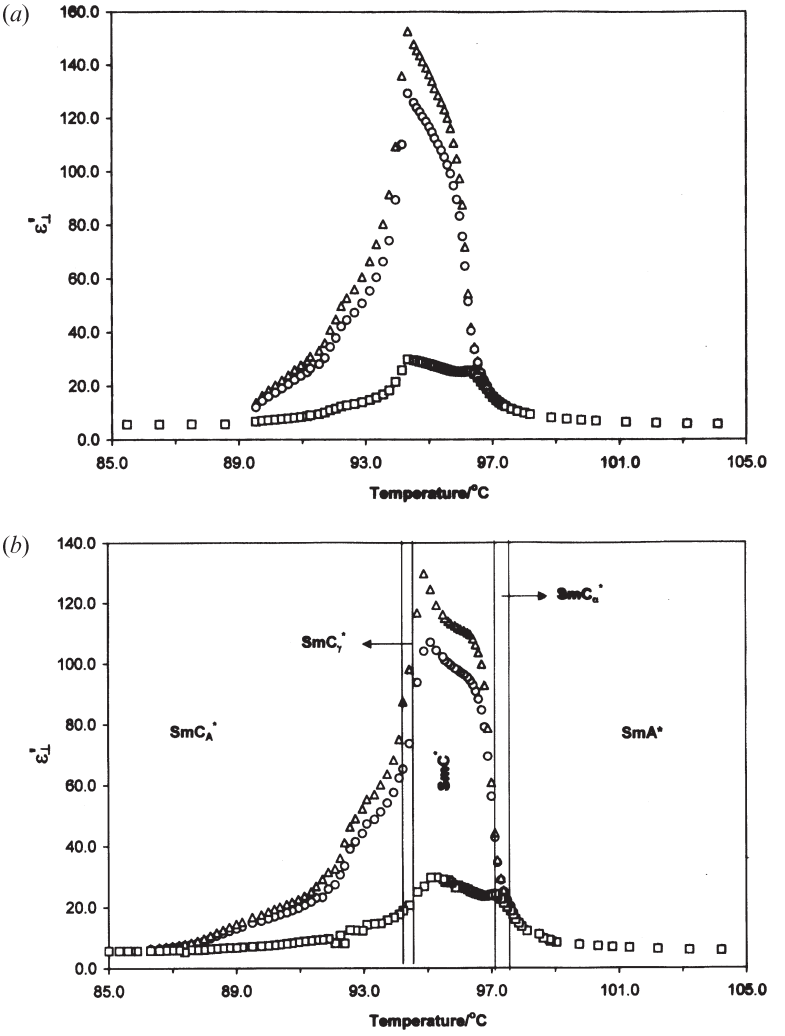

Figure 5. Temperature dependence of the real part of dielectric permittivity $\varepsilon'_\perp$ at three different frequencies: 100 Hz (Δ), 1 kHz (○) and 10 kHz (□) during (*a*) heating and (*b*) cooling cycles. Vertical lines show the separation of different phases on the basis of DSC data and may not represent the exact transitions of dielectric parameters; see text for other details.

mode observed in the SmA* phase increases significantly in the SmC$_\alpha^*$ and SmC* phases. On further cooling, the dielectric strength decreases with decrease in temperature in the SmC$_\gamma^*$ phase. The distribution parameter h calculated with the help of a Cole–Cole plot in the SmA* phase was found to be approximately zero, which indicates that this relaxation mode arises from a single molecular phenomenon; in the case of SmC* subphases, the h lies between 0.15 and 0.25, which shows the quasi-dispersive nature of these subphases [18]. Two relaxation modes observed in the SmC$_A^*$ phase are shown in figure 6 (*f*), from which the dielectric strengths of the two modes were found to be 0.80 and 0.75. The distribution parameter h was found to be approximately 0.12 for the low frequency relaxation mode, and approximately zero for the high frequency relaxation mode.

Temperature dependence of relaxation frequencies f_R and dielectric strengths $\Delta\varepsilon$ in various phases is shown in figures 7 and 8, respectively. In the SmA* phase, one relaxation mode at about 700 kHz becomes visible at about 103°C (~14°C below the I–SmA* transition). The relaxation frequency of this mode shifts towards the lower side on approaching the transition to the SmC$_\alpha^*$ phase, whereas its dielectric strength increases. Taking account of the molecular structure of the SmA* phase and its temperature dependence behaviour, this mode must correspond to an amplitude mode (so-called soft mode) which is associated with director tilt fluctuation of molecules in the smectic layers [15–19]. In some AFLCs, characteristics of the soft mode can be observed more clearly when the compound exhibits a simple phase transition from SmA* to SmC$_A^*$ [5, 9]. No soft mode relaxation in the SmA* phase above 103°C

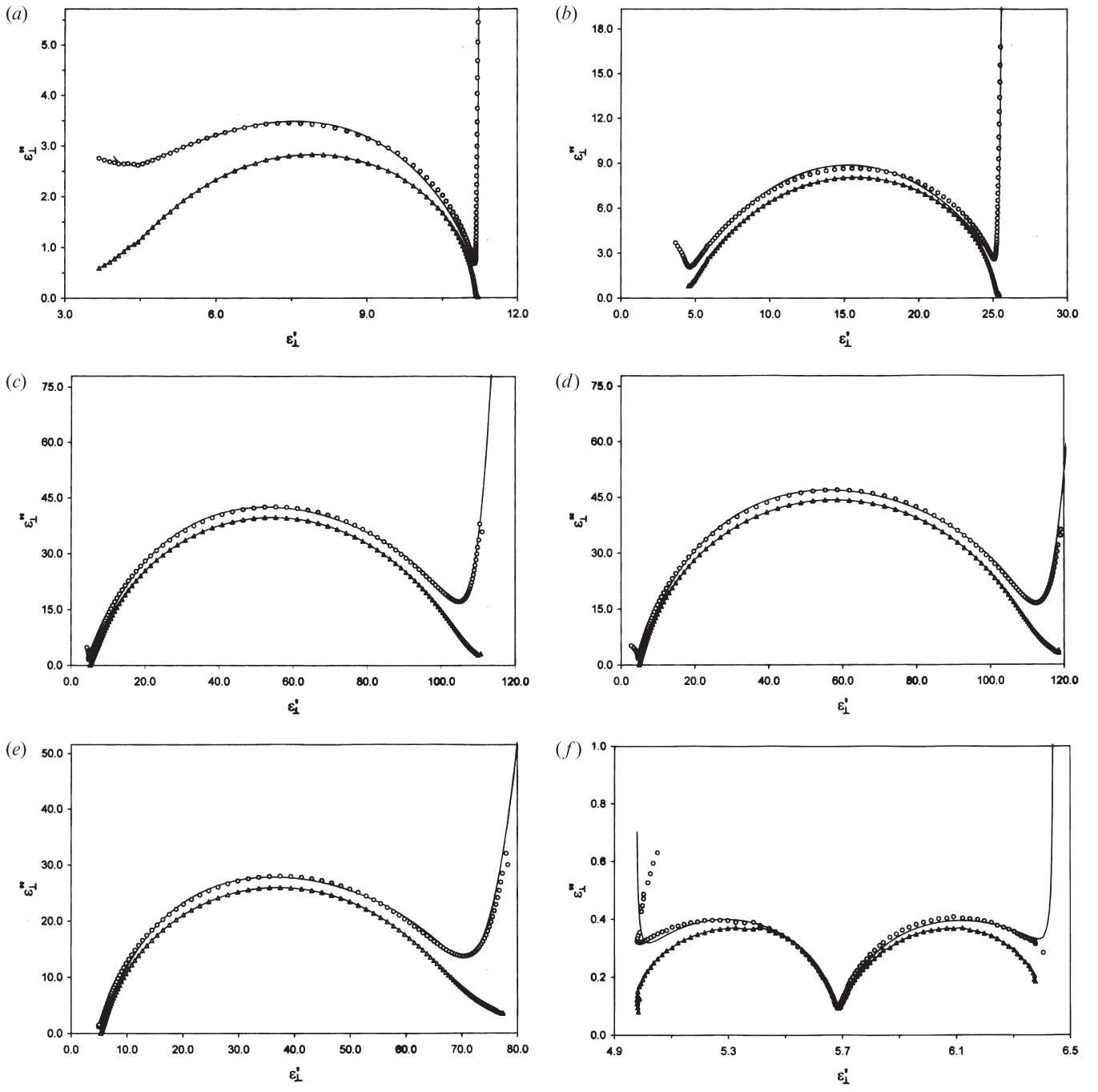

Figure 6. Cole–Cole arcs in (*a*) SmA* phase at 98.5°C, (*b*) SmC^*_α phase at 97.4°C, (*c*) SmC* phase at 96.4°C, (*d*) SmC* phase at 95.5°C, (*e*) SmC^*_γ phases at 94.4°C and (*f*) SmC^*_A phase at 31.8°C. The experimental data and corrected data (experimental data-correction terms) are shown by open circles and triangles, respectively. The solid line with the experimental data shows the best fitting of equation (1); the solid line with the corrected data merely shows the continuity of data points.

could be detected, due to weak dielectric strength and dominating high frequency effect.

A typical dielectric absorption spectrum of the SmC^*_α phase is shown in figure 1 (*b*). The obtained spectrum is well described by a single Cole–Cole type relaxation, see figure 6 (*b*). The relaxation frequency continuously decreases with decrease in temperature while passing through SmA*–SmC^*_α–SmC* transitions (see figure 7). Due to small temperature range of the SmC^*_α phase ($\sim$0.5°C) and large uncertainty in the determination of the relaxation frequencies, it is difficult to isolate the variation of relaxation frequency of

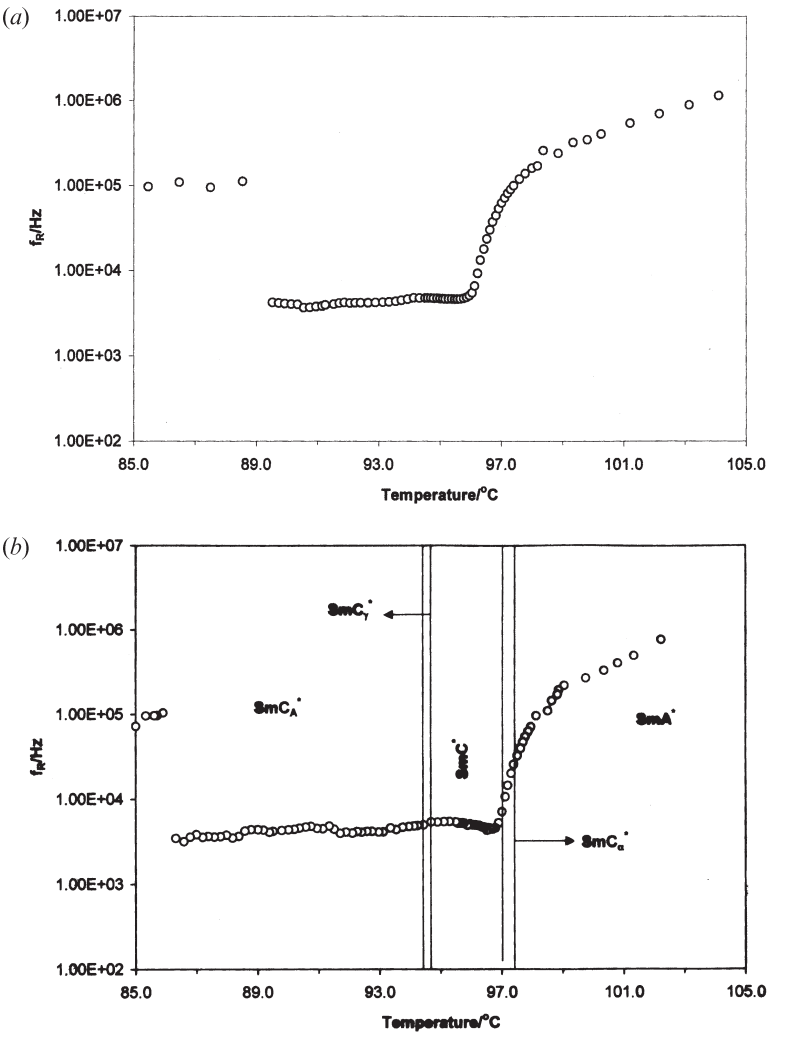

Figure 7. Temperature dependence of the relaxation frequencies of different modes in the SmA*, chiral SmC subphases (SmC$_\alpha^*$, SmC* and SmC$_\gamma^*$) and SmC$_A^*$ phase on an expanded temperature scale during (*a*) heating and (*b*) cooling. Vertical lines show the separation of different phases on the basis of DSC data, which may not represent exact transitions of dielectric parameters.

the SmC$_\alpha^*$ phase from those of the SmA*–SmC* transition; however, there are some fluctuations of relaxation frequency from the smooth variation near the SmC$_\alpha^*$ phase (see figure 7). On cooling the sample, $\Delta\varepsilon$ increases sharply in the SmC$_\alpha^*$ phase (see figure 8). The distribution parameter h was found to be approximately 0.2 for the SmC$_\alpha^*$ phase, which is an indication that this relaxation process is different from the soft mode relaxation seen in the SmA* phase (for SmA* phase $h \sim 0$). Higher value of h in the SmC$_\alpha^*$ phase, i.e. broadening of the relaxation peak as compared with an orthogonal SmA* phase, may be assigned to the tilting of molecules in the SmC$_\alpha^*$ phase.

In other materials (11HFBBM7 [7], MHPOCBC [34], MHP*n*CBC [35]) where the temperature range of the SmC$_\alpha^*$ phase is large ($\sim$3–6°C), the slope for the variation of relaxation frequency of the SmC$_\alpha^*$ phase was found to be different from those of the SmA* and the SmC$_\alpha^*$–SmC* transition region. In these reports, the SmC$_\alpha^*$ relaxation process was assigned as ferroelectric soft mode [7, 34, 35], which seems to be the case in the present sample also. In the case of *R*-MHPOBC, Hou *et al.* [13] have reported two relaxation modes in the SmC$_\alpha^*$ phase, at about 100 and 6 kHz. The high frequency relaxation mode shows the expected slowing down behaviour, while its dielectric strengths increases slightly with decrease in temperature. On the other hand, the lower frequency mode was found to be temperature independent, its dielectric strength increasing sharply with decrease in temperature and reaching about 100 near the SmC$_\alpha^*$–SmC* phase transition. It is attributed to the Goldstone mode on the basis of its

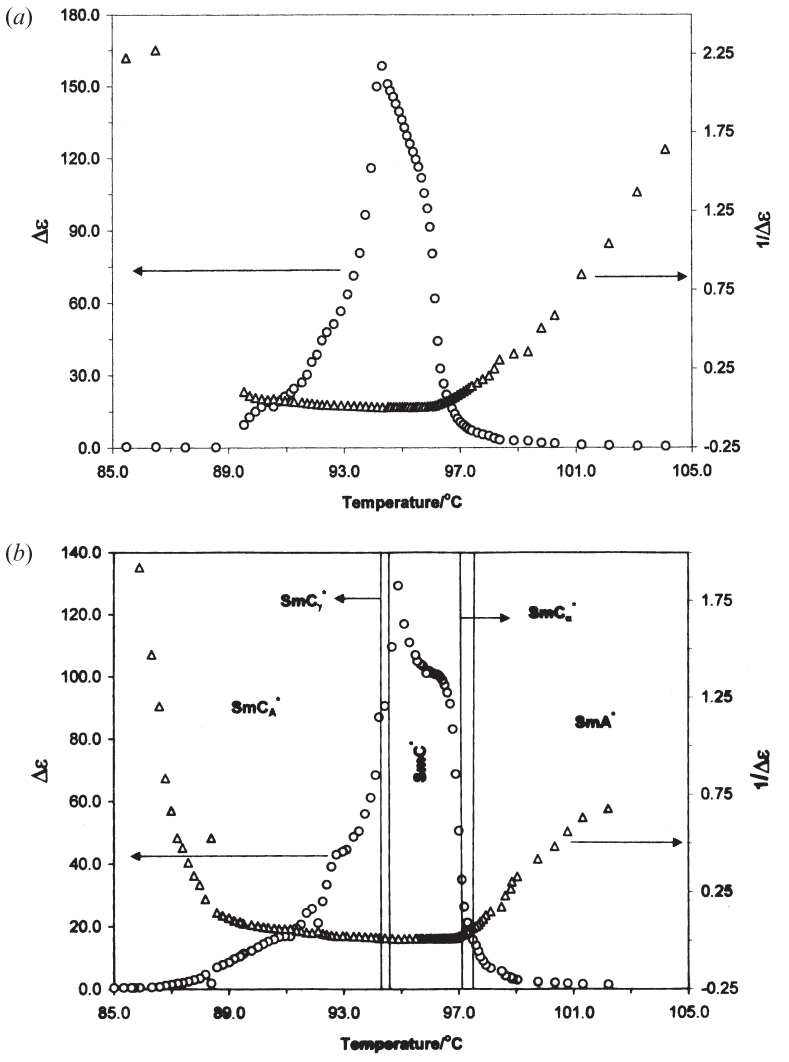

Figure 8. Temperature dependence of dielectric strength $\Delta\varepsilon$ and inverse of dielectric strength $1/\Delta\varepsilon$ in the SmA*, chiral SmC subphases (SmC_α^*, SmC* and SmC_γ^*) and SmC_A^* phases on an expanded temperature scale during (*a*) heating and (*b*) cooling. Vertical lines show the separation of different phases on the basis of DSC data, which may not represent exact transitions of dielectric parameters.

bias field dependence. While fitting the experimental data of the SmC_α^* phase of the present material, it has been observed that one more mode of relaxation may be possible, but due to overlapping of two modes, the presence of correction terms and the weak nature of one relaxation mode, it is difficult to isolate them in the vicinity of the SmC_α^*–SmC* phase transition.

At the transition to the SmC* phase, the relaxation frequency reaches a minimum at about 5 kHz while the dielectric strength shows a diverging nature (see figures 7 and 8). Throughout SmC* phase, f_R remains almost constant whereas $\Delta\varepsilon$ increases and reaches its maximum value near the SmC*–SmC_γ^* transition (see figure 8). This mode has been attributed to the phason mode (also called Goldstone mode) arising due to the precession of tilted molecules around the helicoidal axis [36]. In the case of MHPOBC [13, 15], a phason mode relaxation has been found at about 8 kHz. However other workers [8, 18] have reported a soft mode also in the SmC* phase. The ferroelectric SmC* phase soft mode seems to be masked by the Goldstone mode in the present material. While fitting the experimental data of the SmC* phase, it was observed that one more relaxation mode may be possible around 50 kHz, but could not be clearly determined at all temperatures because of its weak nature. This mode may possibly be a soft mode.

On further cooling, the Goldstone mode of the SmC* phase shifts slightly towards lower frequencies in the SmC_γ^* phase, and its dielectric strength decreases

continuously throughout the phase. However, in the case of MHPOBC [13, 15], two relaxation modes were observed for the SmC^*_γ phase, one at about 1 MHz, the other at about 4 kHz. In the same report it was observed that the dielectric strength and relaxation frequency of the high frequency relaxation mode remain invariant with temperature, and the low frequency mode decreases in strength with decrease in temperature and vanishes near the SmC^*_γ–SmC^*_A phase transition. We were unable to find any such relaxation in the MHz frequency range. Even if it exists, it may be masked by high frequency effects of the dielectric cell. The decrease of dielectric strength in the SmC^*_γ phase, occurs because of the decrease in ferroelectric order (or increase in antiferroelectric order) with decrease in temperature. For ordinary FLCs, the Goldstone mode can be easily observed in the ferroelectric SmC* phase, but in the case of AFLC materials, especially in the case of the ferrielectric SmC^*_γ phase, the situation is quiet different, because in the SmC^*_γ phase molecules may not always fluctuate continuously in the same azimuthal direction on the larger scale, and at some places other types of molecular tilting, with a large phase difference such as anti-tilt pairs, may also exist in neighbouring layers [13]. Locally, the direction configuration can be approximately described by parallel tilt and anti-tilt pairs. The azimuthal angle fluctuation of the anti-tilt pairs usually induces only very small local polarization or none at all [17]. As in the three-layered ferrielectric phase, molecules in the two layers tilt in the same direction whereas in the third layer they tilt in the opposite direction [12, 13]; therefore the effective value of spontaneous polarization in the ferrielectric phase is one third the spontaneous polarization in the ferroelectric phase. Hence the contribution of the Goldstone mode to $\Delta\varepsilon$ in the ferrielectric SmC^*_γ phase is lower than in the ferroelectric SmC* phase.

By analogy with the ferroelectric phase, the dielectric strength $\Delta\varepsilon_G$ and the relaxation frequency f_G of the ferrielectric Goldstone mode can be written as [36]

$$\Delta\varepsilon_G = \frac{1}{2\varepsilon_0 K_\varphi}\left(\frac{\mathbf{P}_s}{q\theta}\right)^2 \tag{3}$$

and

$$f_G = \frac{K_\varphi\, q^2}{2\pi\gamma_\varphi} \tag{4}$$

where $\boldsymbol{K}_\varphi$, γ_φ, P_s, and $\boldsymbol{\theta}$ are the elastic constant, coefficient of rotational viscosity, spontaneous polarization and tilt angle, respectively. $\boldsymbol{q} = (2\pi/\boldsymbol{p})$ is the helical wave vector of pitch $\boldsymbol{p}$. From equation (3), the dielectric strength of the Goldstone mode in the ferrielectric phase is directly proportional to the square of mesoscopic polarization and helical pitch. As the dielectric strength of the Goldstone mode in the SmC^*_γ phase is found to vary with temperature throughout the phase, this behaviour indicates that either one of the parameters mesoscopic polarization and helical pitch, or both, changes drastically with temperature. If the variation is in the mesoscopic polarization then this implies that the three-layer unit cell changes configuration continuously within the SmC^*_γ phase. It has been reported for some materials that helical pitch increases strongly in the SmC^*_γ phase on cooling from the SmC* [12, 21], and we notice the same effect by the optical texture study of our present material and its pitch measurement. Therefore from equation (4) one may speculate that $\boldsymbol{f}_G$ would decrease by about one decade in comparison with the Goldstone mode relaxation frequency of the SmC* phase, if other parameters remain unchanged. But in the present case, the helicoidal structure of the SmC^*_γ phase is supposed to be more rigid than the ferroelectric SmC* phase, resulting in a higher value of $\boldsymbol{K}_\varphi$. Therefore the increase in helical pitch is compensated by a high value of $\boldsymbol{K}_\varphi$ in the SmC^*_γ phase, resulting in only a small change in the relaxation frequency of this mode. In the case of some other AFLCs [8, 19–21], a relaxation mode at several Hz has also been reported.

Cepic *et al*. [21] have proposed another model for the SmC^*_γ phase, on the basis of optical measurements. In this model, three-layer crystallographic units of the SmC^*_γ phase are randomly switched to opposite directions, creating an array of defects along the layer normal which results in the formation of short domains with opposite polarization. Therefore the mode obtained at lower frequency ($\sim$Hz) is related to the movements of domain boundaries. These authors have also reported that even a relatively weak electric field distorts the SmC^*_γ array of defects and produces relatively large domains with nearly uniform polarization, and the Goldstone mode related to the distortion of the helix become more pronounced. The relaxation mode of the SmC^*_γ phase found in the present material occurs at a frequency approximately two decades higher than the frequency reported by Cepic *et al*.; hence it is not reasonable to correlate this mode with movements of domain boundaries.

The SmC^*_γ–SmC^*_A phase transition was recorded by DSC and also detected during texture study, but could not be observed in dielectric studies; however, this is a first order phase transition [2, 12, 13] as evident also from the DSC thermogram (see figure 2). The dielectric spectrum of the SmC^*_A phase contains two characteristic relaxation modes P_L (lower frequency mode) and P_H (higher frequency mode) observed in the kHz and MHz regions, respectively [9–11, 17–19]. The

temperature dependence of the relaxation frequencies and dielectric strengths of the P_L and P_H modes are shown in figures 9 (*a*) and 9 (*b*), respectively. The P_L mode, with relaxation frequency $\sim$90 kHz, was observed at the onset of the SmC_A^* phase, and the dielectric strength of this relaxation mode is quite small in comparison with that of other relaxation modes observed in chiral smectic C subphases. On further cooling, another relaxation mode at about 200 kHz has appeared below 52°C, while during heating this mode survived up to 60°C. The dielectric strengths of both modes were found to be less than unity and vary between 0.40 and 0.90 throughout the phase. The relaxation frequencies of both modes decrease with decrease in temperature and reach about 200 Hz and 58 kHz, respectively, at about 30°C. However in the case of MHPOBC, a single relaxation mode was observed at about 1 MHz with dielectric strength $\sim$6 for the SmC_A^* phase at zero bias field [13] and the other relaxation mode was observed at several kHz with dielectric strength less than unity only after application of a bias electric field. The dielectric strength of the high frequency relaxation mode reported for MHPOBC [13] is large in comparison with other AFLCs studied up to now [9–11, 17–19]. After viewing the dielectric spectra carefully [13], it seems that the position of the high frequency relaxation mode is very close to that of the absorption peak related to cell relaxation. This implies that the high dielectric strength of this mode may be the consequence of an ITO effect. For the same compound, an absorption in the same frequency range has also been reported by Hiraoka *et al.* [15] but with small dielectric strength; in their dielectric cell the relaxation frequency of the cell occurs at about 10 MHz

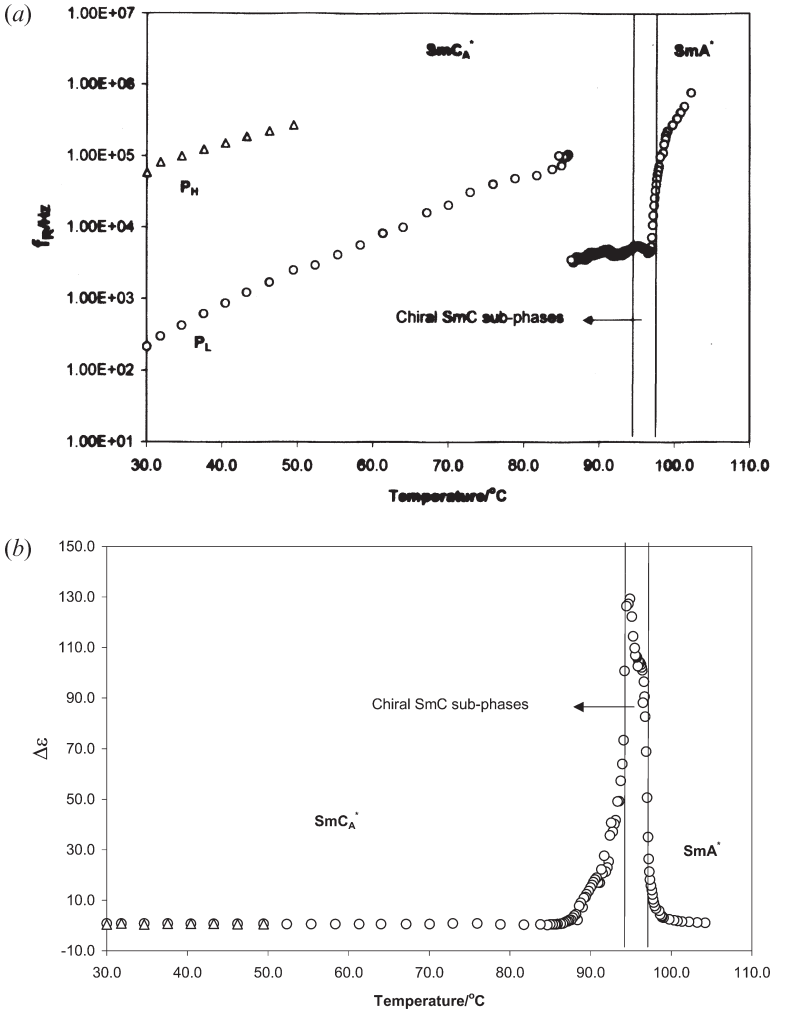

Figure 9. (*a*) Temperature dependence of the relaxation frequencies of different modes in SmA*, chiral SmC subphase and SmC_A^* phases during cooling. (*b*) Temperature dependence of the dielectric strength $\Delta\varepsilon$ of different modes in SmA*, chiral SmC sub-phases, and SmC_A^* phases during cooling.

and hence high frequency effects are small in the observed mode.

The two relaxation modes (P_L and P_H) are considered to be related, respectively, to in-phase and anti-phase azimuthal angle fluctuation of the directors in the anti-tilted molecular pairs [17]. The anti-phase fluctuation at high frequency can cause changes in local polarization and hence is directly detectable, whereas the in-phase fluctuation can be observed only when anti-tilt pairs are distorted. Dielectric studies of the SmC_A^* phase have been carried out by other groups who give similar explanations [10, 13, 18].

In addition to the above two modes in the SmC_A^* phase, a strong absorption peak at about 3 kHz has been observed below the SmC_γ^*–SmC_A^* phase transition (see figure 7). The dielectric strength of this mode is higher by one order of magnitude than those of the P_L and P_H modes, while its relaxation frequency is lower than the P_L and P_H relaxation frequencies. The dielectric strength of this mode decreases with decrease in temperature and it is suppressed below $\sim 8^\circ$C during cooling to the SmC_γ^*–SmC_A^* phase transition. There are reasons to believe that this relaxation mode is uncharacteristic of the SmC_A^* phase because of its high dielectric strength and temperature dependence. The origin of this mode is the coexistence of SmC_γ^* and SmC_A^* phases below the SmC_γ^*–SmC_A^* transition. In general, non-characteristic peaks may appear in adjacent phases due to the coexistence of phases across a first order phase transition [3, 19]. It is thus the Goldstone mode of the ferrielectric SmC_γ^* phase, which penetrates into the antiferroelectric SmC_A^* phase in this case. This may also be a reason that the SmC_γ^*–SmC_A^* phase transition could not be clearly resolved while recording the dielectric spectrum. Hiller *et al.* [16] and Buivydas *et al.* [19] have reported supercooling effects in some other antiferroelectric materials, even up to 15°C. In the case of our present material, one may expect that supercooled polar responses should not be observed during heating. To clarify the point, we performed the heating cycle but only from SmC_A^* phase at room temperature (and not from the crystal phase), as material did not crystallize up to room temperature (18°C). During heating, the Goldstone mode again appeared at about $\sim 6^\circ$C below the SmC_A^*–SmC_γ^* transition. The presence of the Goldstone mode in the SmC_A^* phase during heating (although in a smaller temperature range than to that during cooling) is surprising. The plausible answer is hidden in the fact that heating could be performed only from the SmC_A^* phase and not from crystal phase, and hence the two processes (cooling and heating) are similar.

4. Conclusions

The existence of different types of mesophases, viz. SmA^*, SmC_α^*, SmC^*, SmC_γ^* and SmC_A^*, in chlorinated MHPOBC has been confirmed by DSC, optical texture and dielectric studies. It has become possible to bring down SmC_A^* phase at room temperature, in a single component system, with a wide temperature range of stability. Seven dielectric relaxation modes have been identified in various mesophases. The single relaxation mode observed in the SmA^* phase has been identified as a soft mode on the basis of its temperature dependence. The SmC_α^*, SmC^* and SmC_γ^* phases show only one dielectric relaxation in each phase due to the collective behaviour of molecules. The relaxation process observed in the SmC_α^* phase shows a steep deceleration and grows significantly in strength on cooling. Its origin has been assigned to the ferroelectric soft mode. In the SmC^* and SmC_γ^* phases, Goldstone mode relaxations have been observed. The relaxation frequency of this mode was found to be temperature-independent in both phases, with a value of about 5 kHz. Only a small variation in relaxation frequency was observed near the transition to the ferrielectric SmC_γ^* phase. Two other types of relaxation mode have been observed in the antiferroelectric SmC_A^* phase: one at about 250 kHz, the other at about 90 kHz. These two relaxation modes are considered to be related, respectively, to anti-phase and in-phase azimuthal angle fluctuation of the molecules in anti-tilt pairs. An additional non-characteristic mode was observed in the SmC_A^* phase resulting from the coexistence of the adjacent SmC_γ^* phase. This mode is assigned to a ferrielectric Goldstone mode which penetrates into the SmC_A^* phase.

We thank the University Grants Commission (UGC) and Department of Science and Technology (DST), New Delhi for financial assistance under a research project. One of us (M.B.P.) thanks UGC especially for a research fellowship. We are grateful to Prof. S. L. Srivastava, Physics Department, Allahabad University, Allahabad for valuable comments and suggestions.

References

[1] Chandani, A. D. L., Ouchi, Y., Takezoe, H., Fukuda, A., Terashima, K., Furukawa, K., and Kishi, A., 1989, *Jpn. J. appl. Phys.,* **28,** L 1261; Chandani, A. D. L., Gorecka, E., Ouchi, Y., Takezoe, H., and Fukuda, A., 1989, *Jpn. J. appl. Phys.*, **28,** L 1265.

[2] Musevic, I., Blinc, R., and Zeks, B., 2000, *The Physics of Ferroelectric and Antiferroelectric Liquid Crystals* (Singapore: World Scientific).

[3] Gorecka, E., Pociecha, D., Cepic, M., Zeks, B., and Dabrowski, R., 2002, *Phys. Rev. E.*, **65061 703/1.**

[4] Lagerwall, J. P. F., Rudquist, P., Lagerwall, S. T., and Giebelmann, F., 2003, *Liq. Cryst.*, **30,** 399.

[5] PANDEY, M. B., DHAR, R., AGRAWAL, V. K., and DABROWSKI, R., 2004, *Mol. Cryst. liq. Cryst.* (in the press).
[6] MACH, P., PINDAK, R., LEVELUT, A. M., BAROIS, P., NGUYEN, H. T., HUANG, C. C., and FURENLID, L., 1998, *Phys. Rev. Lett.*, **81,** 1015.
[7] SARMENTO, S., CARVALHO, P. S., CHAVES, M. R., NGUYEN, H. T., and PINTO, F., 1999, *Mol. Cryst. liq. Cryst.*, **328,** 457.
[8] HATANO, J., HANAKAI, Y., FURUE, H., UEHARA, H., SATIO, S., and MURASHIRO, K., 1994, *Jpn. J. appl. Phys.*, **33,** 5498.
[9] UEHARA, H., HANAKAI, Y., HATANO, J., SATIO, S., and MURASHIRO, K., 1995, *Jpn. J. appl. Phys.*, **34,** 5424.
[10] PANARIN, Y. P., KALINOVSKAYA, O., VIJ, J. K., and GOODBY, J. W., 1997, *Phy. Rev. E.*, **55,** 4345.
[11] PANARIN, Y. P., KALINOVSKAYA, O., and VIJ, J. K., 1998, *Liq. Cryst.*, **25,** 241.
[12] TAKEZOE, H., LEE, J., OUCHI, Y., and FUKUDA, A., 1991, *Mol. Cryst. liq. Cryst.*, **202,** 85.
[13] HOU, J., SCHACHT, J., GIEBELMANN, F., and ZUGENMAIER, P., 1997, *Liq. Cryst.*, **22,** 409.
[14] LAGERWALL, S., DAHLGREN, A., JAGEMALM, P., RUDQUIST, P., D'HAVE, K., PAUWELS, H., DABROWSKI, R., and DRZEWINSKI, W., 2001, *Adv. funct. Mater.*, **11,** 87.
[15] HIRAOKA, K., TAGUCHI, A., OUCHI, Y., TAKEZOE, H., and FUKUDA, A., 1990, *Jpn. J. appl. Phys.*, **29,** L103.
[16] HILLER, S., PIKIN, S. A., HASSE, W., GOODBY, J. W., and NISHIYAMA, I., 1994, *Jpn. J. appl. Phys.*, **33,** L1096.
[17] BUIVYDAS, M., GOUDA, F., LAGERWALL, S. T., and STEBLER, B., 1995, *Liq. Cryst.*, **18,** 879.
[18] CARVALHO, P. S., CHAVES, M. R., DESTRADE, C., NGUYEN, H. T., and GLOGAROVA, M., 1996, *Liq. Cryst.*, **21,** 31.
[19] BUIVYDAS, M., GOUDA, F., ANDERSSON, G., LAGERWALL, S. T., STEBLER, B., BOMELBURG, J., HEPPKE, G., and GESTBLOM, B., 1997, *Liq. Cryst.*, **23,** 723.
[20] SHTYKOV, N. M., VIJ, J. K., LEWIS, R. A., HIRD, M., and GOODBY, J. W., 2001, *Liq. Cryst.,* **28,** 1699; GLEESON, H. F., BAYLIS, L., ROBINSON, W. K., MILLS, J. T., GOODBY, J. W., SEED, A., HIRD, M., STRYING, P., ROSENBLATT, C. and ZHANG, S., 1999, *Liq. Cryst*., **26,** 1415.
[21] CEPIC, M., GORECKA, E., POCIECHA, D., ZEKS, B., and NGUYEN, H. T., 2002, *J. chem. Phys.*, **117,** 1817.
[22] MARZEC, M., POPCZYK, J., FAFARA, A., WROBEL, S., and DABROWSKI, R., 2002, *Ferroelectrics*, **281,** 123.
[23] SUWA, S., TAKANISHI, Y., HOSHI, H., ISHIKAWA, K., and TAKEZOE, H., 2003, *Liq. Cryst.*, **30,** 499.
[24] GASOWSKA, J., DABROWSKI, R., DRZEWINSKI, W., FILIPOWICZ, M., PRZEDMOJSKI, J., and KENIG, K., 2004, *Proc. 9th Int. Conf. on Ferroelectric Liquid Crystals,* August 24–29, 2003, Dublin, to be published in *Ferroelectrics* (in the press).
[25] LAGERWALL, J., RUDQUIST, P., LAGERWALL, S., and STEBLER, B., 2002, *Ferroelectrics*, **277,** 239.
[26] FURUKAWA, K., TERASHIMA, K., ICHIHASHI, M., SAITOH, S., MIYAZAWA, K., and INUKAI, T., 1988, *Ferroelectrics*, **85,** 451.
[27] SASAKI, T., and IKEDA, T., 1995, *J. phys. Chem.*, **99,** 13 002.
[28] SRIVASTAVA, S. L., DHAR, R., and KURIK, M. V., 1993, *Mol. Mater.*, **2,** 261.
[29] PANDEY, M. B., DHAR, R., AGRAWAL, V. K., KHARE, R. P., and DABROWSKI, R., 2003, *Phase Transitions*, **76,** 945.
[30] HILL, N. E., VAUGHAN, W. E., PRICE, A. H., and DAVIES, M., 1969, *Dielectric Properties and Molecular Behaviour* (London: Van Nostrand Reinhold).
[31] SRIVASTAVA, S. L., and DHAR, R., 1991, *Indian J. pure appl. phys.*, **29,** 745.
[32] GOUDA, F., SKARP, K., and LAGERWALL, S. T., 1991, *Ferroelectrics*, **113,** 165.
[33] SRIVASTAVA, S. L., 1993, *Proc. nat. Acad. Sci. India*, **63,** 311; DHAR, R., 2004, *Indian J. pure appl. Phys*., **42**, 56.
[34] KIMURA, Y., and HAYAKAWA, R., 2002, *Eur. Phys. J. E.*, **9,** 3.
[35] CEPIC, M., HEPPKE, G., HOLLIDT, J. M., LOTZSCH, D., MORO, D., and ZEKS, B., 1995, *Mol. Cryst. liq. Cryst.*, **263,** 207.
[36] LEVSTIK, A., CARLSSON, T., FILIPIC, C., LEVSTIK, I., and ZEKS, B., 1987, *Phys. Rev. A*, **35,** 3527.